CO_2 photoreduction with water: Catalyst and process investigation

A. Olivo[a], V. Trevisan[a], E. Ghedini[a], F. Pinna[a], C.L. Bianchi[b], A. Naldoni[c], G. Cruciani[d], M. Signoretto[a,*]

[a] Dept of Molecular Sciences and Nanosystems, Ca'Foscari University Venice and INSTM Consortium, RU of Venice, Dorsoduro 2137, 30123 Venezia, Italy
[b] Dept. of Chemistry, Milan University and INSTM Consortium, RU of Milano, Via Golgi 19, 20133 Milan, Italy
[c] CNR-Istituto di Scienze e Tecnologie Molecolari, Via Golgi 19, 20133 Milano, Italy
[d] Dept. of Physics and Earth Sciences, University of Ferrara, Via G. Saragat 1, I-44122 Ferrara, Italy

ARTICLE INFO

ABSTRACT

Economic development should not be separated from the concept of sustainability. The goal can be pursued by means of technologically advanced materials and processes that enable environmental protection. Carbon dioxide photoreduction using water as reducing agent could be a green and effective way to pursue this aim and titania is a good photocatalyst for this reaction. In this work the performances of N doped CuO–TiO$_2$ photocatalysts in gas phase CO_2 reduction have been studied. We have focused the attention on both the catalysts design and the process optimization. We have investigated, in particular, the effect of the presence of nitrogen and copper amount on the final catalysts performances. In order to learn high control of the catalytic process and to manage productivity and selectivity, by operating in very mild reaction conditions, the last part of the work has been centered on tuning the process parameters (CO_2/H_2O ratio). It has been observed that the CH_4 formation is sensitive to copper amount and that exists a close correlation between the catalytic behavior and the reagents ratio.

1. Introduction

It is well known that climate has rapidly changed in the last decades in terms of average temperatures and severity of weather phenomena [1,2]. Though climate variability is common and natural in geological history, nowadays it definitely has an anthropogenic boost [3]. The main driving force in climate change is the increasing concentration of greenhouse gases (GHGs) [4]. Among them, carbon dioxide emissions are the most abundant [5]: the International Environmental Agency (IEA) stated that in 2012 CO_2 emissions reached 31.6 Gt [6]. Since the beginning of the industrial era, average CO_2 concentration in atmosphere increased from 270 ppm to 400 ppm in May 2013 [7]. This trends are dependent on fossil fuels utilization and our economic system strongly relies on carbon-based energy technologies [8]. Therefore the two most challenging issues of the 21st century, that are CO_2 increasing emissions and fossil fuels depletion, are strictly connected one to another. So it is extremely important to transform this pollutant into products whose market have worldwide dimensions, i.e. fuels [9]. The inspiration for this approach comes from nature: [10] planet Earth balanced its atmosphere composition by itself for thousands, if not millions of years by means of photosynthesis. With this natural process, plants transform water and carbon dioxide into the high energy molecules they need for living. A similar approach is believed to be a winning solution to the environmental problem. In literature, many works focus on the so-called "artificial photosynthesis" [11,12]. The similarity is that in both cases light is the primary energy source and high energy products are formed; on the other hand, typical artificial systems are completely different from natural ones [11]. Common products are gaseous and liquid fuels, as reported in Eq. (1).

$$x\ CO_2 + y\ H_2O + h\nu \rightarrow solar\ fuels + z\ O_2 \quad (1)$$
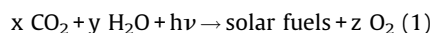
They can be readily used in stationary and mobile applications, since they are equivalent to the fossil ones. Differently from traditional fuels, carbon dioxide from solar hydrocarbons combustion can be recycled, closing carbon circle by means of a non-biological process [11]. Moreover, solar fuels distribution is compatible with already present infrastructures for fossil hydrocarbons [13,14]. For all these reasons, photocatalysis appears to be an attractive technology to pursue carbon dioxide photoreduction [15–17]. In this work the attention has been addressed to photoreduction of carbon dioxide using water as reducing agent [18–21] (Eq. (2)).

$$CO_2 + 2\ H_2O \rightarrow CH_4 + 2\ O_2 \quad \Delta H° = +802\ kJ/mol \quad (2)$$
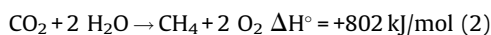
As a catalyst, titania has been chosen. This material is nontoxic and inexpensive, and it has good photocatalytic properties [22–27]. It has been already applied to several environmental and energetic applications, like water splitting [28], VOC [29,30] and NOx abatement [31–33]. Inoue et al. [34] first reported that titania is able to catalyse CO_2 photoreduction with water. In fact, when irradiated, a charge separation is generated and the electron-hole pair is formed [35]: in the valence band, oxygen from water is oxidized to molecular oxygen while the excited electron reduces carbon from CO_2 releasing oxygen as well [36,37]. Then protons and reduced carbon react together generating the desired product [38].

Other stable compounds (such as CO, formic acid, formaldehyde and methanol) might be produced in this process but reaction pathway and process selectivity are highly dependent on light absorption, creation of charge carriers and their use in the process [39,40].

Unfortunately, the relatively fast recombination rate of photoinduced electron-hole pairs and a low quantum yield for oxygen production as a result of the UV photons absorption restrict the potential photo-application of TiO_2. To overcome these drawbacks, many efforts have been carried out including deposition of noble metals, dye sensitization, metal cation doping, carbon and nitrogen doping [24] and morphology and structure control [41]. Positive effects on titania photoactivity can be pursued by doping with non-metal elements like boron [42], carbon [43], nitrogen [44], fluorine [45] and iodine [46]. These dopants can either substitute oxygen in titanium dioxide lattice or occupy interstitial sites [47]. In both cases, a red shift in titania light adsorption is observed due to a decrease in band gap energy. Among non-metal dopants, nitrogen is one of the most investigated [48]. The incorporation of this element in titanium dioxide lattice causes several electronic modifications that are responsible for enhanced photoactivity: in particular, doping introduces intra band gap electronic states that cause a decrease in required energy for photoexcitation [49]. In addition to that, doping with several noble metals were tested like platinum [50], silver [51] and gold [52,53] that stabilize the separation of photoexcited charge carriers. Generally, metal loading is very low, usually less than 1 wt.% [54]: high metal fractions are detrimental to titanium dioxide photoactivity [55]. Greater attention has been put on less precious transition metals as Fe and Cu. The incorporation of transition metal ions (e.g., Cu^{2+}, Cu^+, Fe^{3+}, etc.) can lead to the formation of electron trapping sites and promote charge transfer from TiO_2 to metal ions, thus resulting in the enhanced photoreaction of surface adsorbed species. Among the transition metal ions, Cu is an appealing dopant due to low cost, availability and enhancement of photoactivity, especially in CO_2 photoreduction. The formation of *pn* junction between Cu and TiO_2 is considered as the major reason for the improvement [56,57]. For heterojunctions with mixed semiconductors, the difference between band edges is the major driving force to improve the charge transfer and subsequently the photocatalytic performance. There have been some studies carried out on the Cu_2O/TiO_2 systems, which have confirmed that this system could enhance the charge separation efficiency and lead to a high photocatalytic activity. Lalitha et al. reported that Cu_2O/TiO_2 nanocomposites with size about 20–40 nm exhibited higher activity than pure TiO_2 in the H_2 evolution [58]; Chu et al. synthesized a Cu_2O/TiO_2 catalyst that showed an excellent photocatalytic activity in 4-nitrophenol degradation [59]. Xu et al. [60] suggested that the Cu (identified as Cu^+) species deposited on TiO_2, forming Ti–O–Cu surface bonds, served as acceptors of electrons that were transferred from the TiO_2 conduction band. Doping with Au or Ag nanoparticles or clusters the sensitivity of the photocatalyst to the visible spectrum can also extend due to their localized surface plasmonic resonance properties [61]. Nevertheless, Cu-loaded TiO_2 catalyst compared to Ag–TiO_2 photocatalysts show higher photoactivity since Cu particles act as electron trapping sites while still maintaining the mobility of photoelectrons [62]. Catalytic reduction of CO_2 with H_2O in the gaseous phase is further investigated by using Cu–Fe/TiO_2 catalyst coated on optical fibres [63]. The synergistic presence of Fe as a co-dopant in Cu/TiO_2 catalyst is has been evidenced in reduction of CO_2 with H_2O to ethylene at the quantum yield and total energy efficiency of 0.024% and 0.016%, respectively. While metal ion modifications of TiO_2 lead to enhancements in charge separation, their effects in altering the optical properties of TiO_2 are limited. In order to overcome this limit, co-doped titania photocatalysts have been studied [64]: in this way electron-hole lifetime is lengthened and visible light adsorption is shifted toward visible light. The used metals are usually noble ones (platinum, gold and silver [65]) while nitrogen is preferred among the non-metallic promoters [66]. So it would be a definite breakthrough to couple a non metal dopant like nitrogen to a less noble metal, like copper.

Catalyst tailoring aside, reaction design conditions must be carefully considered. Fluidized bed reactor is the most common photoreactor [67]. It is employed for batch processes in two-phase heterogeneous systems and generally the catalyst is suspended in an aqueous medium. For this reason the main drawback is CO_2's poor solubility in water [68]. Otherwise, many studies employ photoelectrochemical (PEC) reactors for gas phase reduction but an external electrical energy must be supplied [67]. Moreover, water adsorption on titania is generally more likely to happen compared to CO_2 [69], though both have to interact on the catalytic surface for CO_2 photoreduction to take place. In fact, on titania surface, water splitting reaction might also occur [70]. Other limits of this system are the low surface area and the complicated separation process required to isolate the catalyst grains. To overcome these drawbacks a valid alternative could be the use of a fixed bed reactor using gaseous reactants. In literature only few examples of gaseous CO_2 photoreduction are reported and the reaction is carried out by using hard conditions in order to implement the final productivity. As a matter of fact, high temperature (up to 100 °C), pressures and irradiance (up to 500 W m^{-2}) are suitable to improve photoactivity [63,71,72], though this choice makes the process more expensive and less sustainable. Moreover, the majority of the reported works employs batch processes in liquid phase. The novelty of this work is the use of N doped CuO-TiO_2 photocatalysts for CO_2 photoreduction in gas phase and under the mildest conditions (i.e. room temperature and atmospheric pressure and low irradiance) in order to overcome all the issues rising from the utilization of liquid phase systems. Therefore, in this work a green, innovative and effective technology for photocatalytic CO_2 abatement and transformation into fuels has been reported. Particular interest has been centred on the catalyst design considering the formulation of several N doped CuO–TiO_2 photocatalysts. At the best of our knowledge, only a few works focus the attention to co-promoted photocatalysts for CO_2 photoreduction; in particular, literature lacks information about N doped CuO–TiO_2 photocatalysts for this process in mild conditions, though these materials might be suitable to this purpose. The physico-chemical features of the catalysts and the process parameters (CO_2/H_2O ratio) will be analyzed and discussed in depth by correlating synthesis, characterizations and reactivity tests.

2. Experimental

2.1. Catalysts synthesis

The following reagents were used as received: $TiOSO_4 xH_2O$ yH_2SO_4 (Ti assay >29%, Sigma–Aldrich), ammonium hydroxide solution (33%, Riedel-de-Haen), sodium hydroxide (assay >97%,

Carlo Erba) and $Cu(NO_3)_2$ $3H_2O$ (assay >99%, Sigma–Aldrich). A standard TiO_2 reference material has been purchased by Euro Support s.r.o. It has been chosen to use this commercial sample as a reference since it is a titanium dioxide characterised by a wide surface area (339 m²/g) and anatase as crystalline phase.

All the samples have been prepared by precipitation method maintaining pH constant and equal to 7. In a typical synthesis, a 1.2 M titanyl sulphate solution and a 9.0 M ammonia solution have been added drop wise and simultaneously to 200 mL of distilled water under vigorous stirring, in order to keep the desired pH. In this way the precipitation agent acts as nitrogen source as well. The $Ti(OH)_4$ suspension has been aged at 60 °C for 20 h. Afterwards, the precipitated has been filtered, and washed with distilled water to remove sulphate ions. The absence of sulphates has been verified by means of barium chloride test [73]. Wet $Ti(OH)_4$ has been dried overnight at 110 °C and calcined at 400 °C for 4 h in air flow. This sample has been labelled NT where N indicates the precipitating agent (ammonia solution) and T stands for titanium dioxide. Nitrogen amount in all the samples is 0.4 wt.% as previously reported [32].

Different amounts of copper have been introduced by means of incipient wetness impregnation using copper nitrate trihydrated before calcination: the chosen metal amounts are: 0.1, 0.2, 0.4 and 0.6 wt.% Cu/TiO_2 ratio. The sample obtained are labelled 0.1CuNT, 0.2CuNT, 0.4CuNT and 0.6CuNT respectively: the number represents the wt.% amount of metal.

Using the same methodology, a nitrogen-free sample has been synthesized using NaOH 9.0 M solution as a precipitation agent. This sample has been labelled NaT, where Na stands for the precipitating agent.

2.2. Catalysts characterization

Thermal analyses (TG/DTA) were performed on a NETZSCH STA 409 PC/PG instrument in air flux (20 mL/min) using a temperature rate set at 5 °C/min in the 25–800 °C temperature range.

X-Ray Diffraction (XRD) patterns of the samples were collected employing a Bruker D8 Advance powder diffractometer with a sealed X-ray tube (copper anode; operating conditions, 40 kV and 40 mA) and a Si(Li) solid state detector (Sol-X) set to discriminate the Cu Kα radiation. Apertures of divergence, receiving and detector slits were 2.0 mm, 2.0 mm, and 0.2 mm respectively. Data scans were performed in the 2θ range 5–75° with 0.02° stepsize and counting times of 3 s/step. Quantitative phase analysis and crystallite size determination were performed by the Rietveld method as implemented in the TOPAS v.4 program (Bruker AXS) using the fundamental parameters approach for line-profile fitting. The determination of crystallite size was accomplished by the Double-Voigt approach and calculated as volume-weighted mean column heights based on integral breadths of peaks.

N_2 adsorption–desorption isotherms at −196 °C were performed using a MICROMERITICS ASAP 2000 analyzer in order to obtain information on surface area and pore volume. Prior to N_2 physisorption experiments, all samples were outgassed at 200 °C for 2 h. Mesopore volume was measured as the adsorbed amount of N_2 after capillary condensation. Surface area was calculated using the standard BET [74] equation method and pore size distribution was elaborated using the BJH method applied to the isotherms desorption branch [75].

The real copper amount of co-doped catalysts was determined by flame atomic absorption spectroscopy (FAAS) after microwave dissolution of the samples using a PerkinElmer Analyst 100. The amount of nitrogen was obtained by elemental analyses with a Carlo Erba CNS Autoanalyser, mod. NA 1500. All analyses were replicated 2–3 times and the precision was >95%.

TPR experiments were carried out in a lab-made equipment: samples (50 mg) were heated at 10 °C/min from 25 °C to 800 °C in a 5% H_2/Ar reducing mixture (40 mL/min STP). The effluent gases were analyzed by a Gow-Mac TCD detector using a magnesium perchlorate trap to stop H_2O.

Diffuse reflectance spectroscopy (DRS) of carefully ground powders was performed with a Thermo Scientific Evolution 600 spectrophotometer, equipped with a diffuse reflectance accessory Praying–Mantis sampling kit (Harrick Scientific Products, USA). A Spectralon® disk was used as reference material. The experimental absorption versus lambda plot was elaborated using the Kubelka–Munk function [76]. The band gap energy (E_g) of the catalysts are determined by the intercept of a linear fit to the absorption edge and they can be estimated using the standard equation, which is based on the relationship between frequency (c/λ) and photon energy ($E_g = 1240/\lambda$).

XPS Surface characterization was performed by means of an XPS instrument (M-Probe—SSI) equipped with a monochromatic Al Kα source (1486.6 eV) with a spot size of 200×750 μm and a pass energy of 25 eV, providing a resolution for 0.74 eV. For all the samples, the C1s peak level was taken as internal reference at 284.6 eV. The accuracy of the reported binding energies (BE) can be estimated to be ±0.2 eV. The quantitative data were also accurately checked and reproduced several times and the percentages error is estimated to be ±1% thanks for a severe confidence in spectral decomposition.

(High-Resolution) Transmission electron microscopy (HR–TEM) images were obtained employing a JEOL JEM 3010UHR (300 kV) TEM, equipped with a single crystal LaB_6 filament and an Oxford INCA Energy TEM 200 energy dispersive X-ray (EDX) detector. All samples were dry deposited on Cu "holey" carbon grids (200 mesh).

2.3. Catalytic tests

Carbon dioxide photoreduction reactions have been carried out in a borate glass tubular fixed bed reactor (diameter 4 mm, length 40 mm) using in each test 400 mg of sample, that have been previously pressed, ground and sieved to 50–70 mesh (0.2–0.3 mm). Catalysts have been loaded and left under a 2 mL/min helium flow for 20 h in order to induce the desorption of adsorbed molecules from atmosphere.

Samples have been lighted using a 125 W mercury UVA lamp (emission range 315–400 nm has been shielded by a special tubolar quartz, purchased from Helios Italquartz s.r.l., to select the wavelength of 366 nm), with an average irradiance of 50 W/m², controlled with a Delta Ohm HD 2302.0 photo-radiometer and a LP 471 probe. In a preliminary test, it has been carefully considered light absorption provided by the reactor itself. It has been observed that irradiance in front of the reactor is the same as behind it: thus it is possible to state that the reactor walls not adsorb the light.

Afterwards, a gaseous mixture of carbon dioxide and water has flown through the reactor. Compressed CO_2 (99.99%) regulated by a mass flow controller was carried through a water bubbler kept at 40 °C to generate CO_2 and H_2O vapour mixture (13.3CO_2/H_2O molar ratio). When the system reached the equilibrium state, the reactor was closed and this was taken as the beginning of the reaction. In other terms, the reaction is not performed under a continuous gas flow, but it takes place in static conditions. Within the sealed reactor, there are 9.2 μmol of CO_2 and 0.7 μmol of H_2O.

The reaction has been monitored for 2, 4 and 6 h. Reaction products have been analyzed by a gas chromatograph (HP G1540A) equipped with a Porapak Q column and a TCD detector. Analysis conditions have been carefully tuned in order to deliver a good separation of reagents and products and in all the analyses,

reagents and products amount is above detection and quantification limits.

Activity results are expressed in turn over numbers (TONs) in $nmol_{CH4}/g_{cat}$, as commonly used in literature [77,78].

In order to study the reaction conditions the carbon dioxide mass flow has been reduced and the water vapour flow has been preserved. To do so, CO_2 has been diluted with an inert (helium) in order to keep total gas mixture flow constant: in this way, temperature in H_2O saturator has not been changed. The tested CO_2/H_2O ratios have been reported in the chart below.

3. Results and discussion

Prior to CO_2 photoreduction activity test, a series of preliminary analyses have been conducted in order to verify the quality of our results. Experiments in which the reduction of CO_2 with H_2O was performed in the dark with photocatalyst or under irradiation in absence of photocatalyst were carried out and the results show that neither CH_4 nor CO were detected.

3.1. N doping effect

Firstly, the effect of nitrogen doping has been investigated. To do so, NT, NaT and the commercial system have been tested for carbon dioxide photoreduction. Productivity after 2, 4 and 6 h reaction has been reported in Figs. 1 and 2.

Under the selected reaction conditions (13.3 CO_2/H_2O feed ratio), a complete selectivity to methane and a continuous increase in methane production along with reaction time has been observed for all the samples. Nitrogen affects positively the catalytic behaviour; in fact, NT system provides the best performance comparing to the nitrogen-free (NaT) and the commercial sample. Before considering a comparison of these results with already published works [19], it must be considered that experimental conditions are considerably milder than those from the few literature works where CO_2 photoreduction is performed in gas phase. Thus, a comparison with literature data would make a little sense.

With the aim to investigate in depth the catalytic results several characterization techniques have been applied.

Surface properties have been investigated by means of nitrogen physisorption and the results are reported in Tables 1 and 2.

All samples are mesoporous with specific surface area higher than $100 m^2/g$. Generally, a high surface area value is greatly desirable for catalysts because it is associated with a great number of superficial active sites. This enhances substrates adsorption on the catalytic surface [79]. For the tested systems, this parameter seems to be significant but not essential to explain the activity results. In fact, commercial TiO_2 shows the highest surface area but not the best catalytic activity.

Considering crystal properties and crystallite sizes, XRD analyses have been performed. Among the TiO_2 crystal structures, anatase seems to be the most advantageous, since the electron-
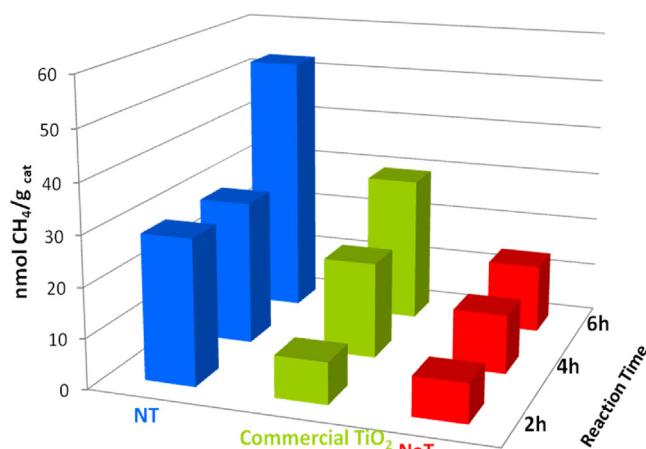

Fig. 2. Production of CH_4 for NT and Commercial TiO_2 in 2, 4 and 6 h.

Table 1
CO_2/H_2O ratios.

CO_2/H_2O	CO_2 μmol	He μmol	H_2O μmol
13.3	9.2	0	0.7
10	7	2.2	0.7
5	5.4	3.8	0.7
2.5	2.6	6.6	0.7
2	1.4	0.8	0.7
1	0.7	8.5	0.7

Table 2
BET surface areas and average pore diameter.

Sample	Surface area m^2/g	Average pore diameter Nm
Commercial TiO_2	339	8
NaT	130	19
NT	110	17

hole recombination is slower in this phase than in rutile and brookite [80].

XRD patterns for the three systems are reported in Fig. 3 and confirm the presence of anatase as the only crystalline TiO_2 phase in all the analyzed systems.

On the other hand, the three samples show some differences in terms of anatase crystal size and sample crystallinity. The XRD bands of the reference TiO_2 are much wider than those of the other two samples due to the smaller crystal size. Furthermore, this sample is characterised by the coexistence of anatase phase (35–40 wt.%) with a large fraction of amorphous titania [81]. This could partially explain the worst catalytic performance of this catalyst compared to NT activity. On the contrary, NT and NaT samples exhibit the typical profile of highly crystalline systems with crystallites size in the range of 8–10 nm. The differences in these
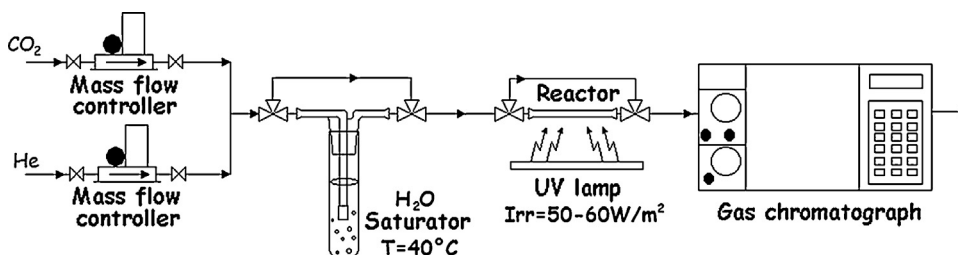

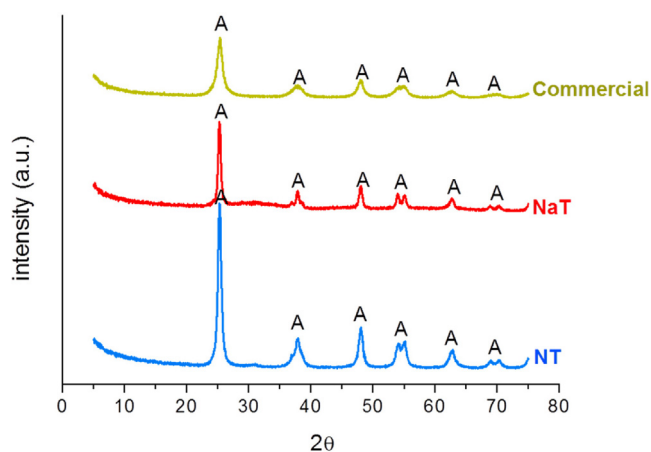Fig. 1. Experimental setup for CO_2 photoreduction.

Fig. 3. Commercial TiO_2, NaT and NT XRD patterns.

two samples found by XRD analyses do not provide a satisfactory explanation for the observed differences in photoactivity. Unfortunately, also XPS spectra do not show any difference between the samples. This means that there are not any species of nitrogen on catalytic surface and any consideration can be made on this matter.

In order to shed some light on the catalytic results, the electronic properties of the samples have been investigated by Diffuse Reflectance Spectroscopy (DRS): a detail of the apparent band gap energy has been reported in Fig. 4.

Considering the absorption spectra in the region between 300 and 500 nm, it is possible to observe that commercial TiO_2 and NaT provide only a well-defined absorption from 390 nm to lower wavelengths, ascribable to the band gap titania photoexcitation. On the other hand, NT shows another wider and less intense absorption band between 390 and 500 nm (see the inset in Fig. 4). The shift of light absorption covering now also the visible region is associated with the presence of nitrogen in titanium dioxide lattice. As reported by Dozzi et al. [47], nitrogen can either occupy lattice positions or interstitial sites. When nitrogen substitutes oxygen in lattice positions, N 2p states are mixed with O 2p ones and adsorption edge from O $2p_\pi$ to Ti d_{xy} is replaced by that from N $2p_\pi$, which requires a lower energy [82]. Nitrogen can occupy also interstitial positions, favouring oxygen vacancies and inducing localized N 2p states within the band gap above the valence band [83]: this also causes shift in light adsorption. In particular this band edge effect, the high adsorption in the UV–vis region, could
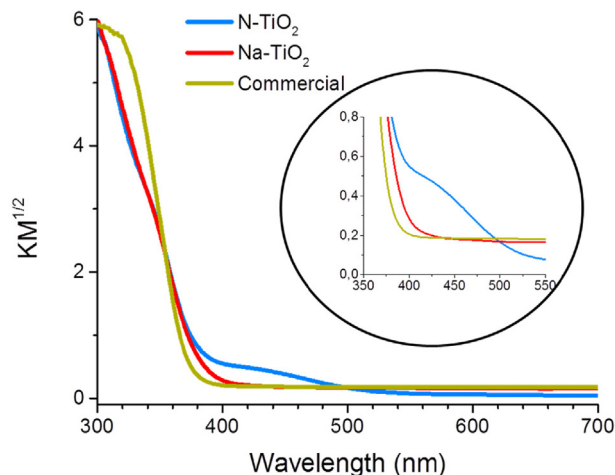
be the reason of the highest activity of the N-doped sample in the carbon dioxide photoreduction.

From DRS spectra, band gap values have been calculated: commercial TiO_2 shows a band gap of 3.25 eV while NaT shows a 3.21 eV band gap in accordance with reference works [84]. Differently, NT shows a lower band bap of 3.16 eV: this means that energy radiation required for light absorption on NT is slightly lower in comparison with NaT and the commercial sample.

From these experimental evidences, we can assume that the role of surface area and crystalline phase are important but not decisive: commercial TiO_2 shows the highest surface area but lower catalytic activity of NT. Only the optimal synergy between texture, crystalline structure and electronic properties provides good catalytic performances; a lead role is played by the electronic state configuration. In particular, in NT, nitrogen introduction modifies titania light absorption and this feature is reflected in its better catalytic performances.

3.2. N doped CuO–TiO2 catalysts

In order to provide a further improvement in catalytic performances, CuO has been added to NT systems as a co-catalyst. CuO has been selected because of its several advantages. Copper acts as a trap not only for electrons but also for holes and the energy levels introduced by impurities are near to CB and VB of TiO_2 as well. Therefore, Cu^{2+} ions presence could be recommended for enhancement of photocatalytic activity [77,85]. Moreover, such electron–hole exchange could also occur between CuO and TiO_2, slowing charges recombination. In this way, the probability of electron transfer to adsorbed CO_2 is increased and then the generation of reactive intermediates such as $•CO_2^-$ and $HCOO^-$ [57,86] is more probable. Copper does not only possess the required features to improve photoactivity of TiO_2, but also it is easily available and inexpensive in comparison with noble metals (Au, Pt, Rh..) and it appears an appealing metal dopant.

The first investigated system is 0.2CuNT, in which Cu loading is 0.2 wt.% (determined by FAAS), in accord with Wu et al. [87].

The sample has been calcined at 400 °C in order to eliminate all the nitrates species derived from copper precursor. In fact, as shown in TG/DTA analysis (Fig. 5), nitrates decomposition is an exothermic process that occurs between 270 °C and 350 °C. Moreover, calcination at 400 °C is aimed at titania phase transition from amorphous to anatase. This process is represented by an exothermic narrow peak between 350 °C and 450 °C in DTA curve, without any weight loss.

After these preliminary considerations, 0.2CuNT has been tested for CO_2 photoreduction. In Fig. 6 the methane production

Fig. 4. NT, NaT and Commercial TiO_2 DRS spectra. In the inset a detail of UV–vis region.
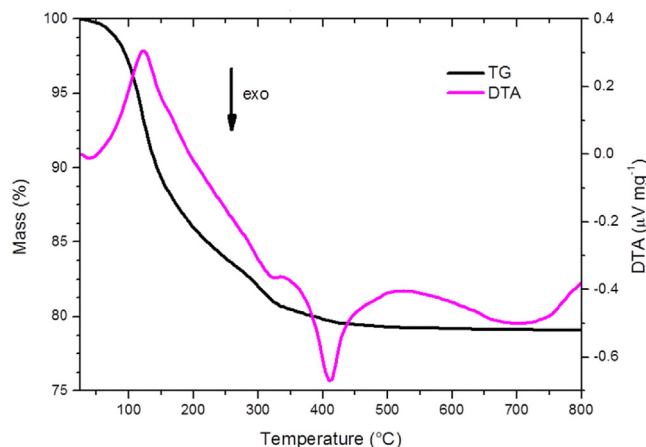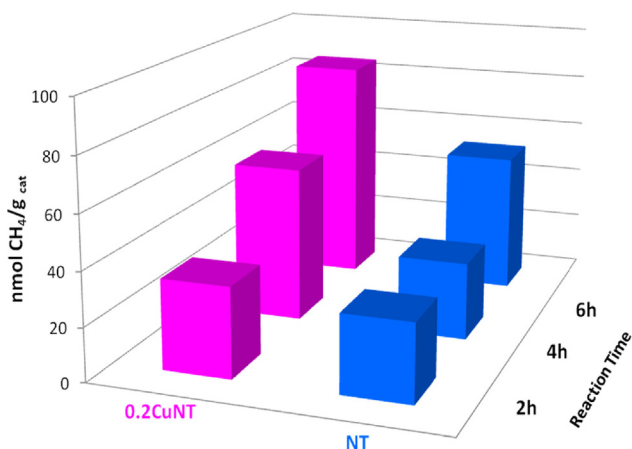

Fig. 5. 0.2CuNT TG/DTA analyses.

Fig. 6. NT and 0.2CuNT trends in methane production.

after 2, 4 and 6 hour of reaction is reported and it has been compared with that obtained with NT sample. It is remarkable that, also in this case, methane is the only detected product for all the catalytic tests.

Copper introduction has a beneficial effect on titania performances in CO_2 photoreduction causing an increase of about 40–50% in methane production after 4 and 6 h.

As revealed by a preliminary characterization, Cu introduction has almost no influence on the resulting texture (surface area and porosity) of the oxide materials, neither it produces relevant structural differences (only anatase crystal phase has been detected also in the 0.2CuNT sample both by XRD analysis and by HRTEM images). Also the XPS spectra are inconclusive to understand the catalytic behaviour of the samples, since there are no substantial differences and the presence of copper species is not revealed due to its low content in the samples. So it would be definitely important to understand more deeply the role that copper covers on the final catalyst. Also in this case, an important answer to this issue has been given by DRS spectra in Fig. 7.

Between 700 and 800 nm (section A), 0.2CuNT exhibits a broad absorption band, that is not present in NT spectrum. This phenomenon is due to the presence of copper and it is related to the photoexcitation of D-electrons from the dopant [88]. Since copper oxides conduction band energy are slightly lower than titania (CuO = 1.6 eV and Cu_2O = 2.4 eV) [76], excited electron can be transferred from TiO_2 conduction band to Cu oxide one: this phenomenon stabilizes the electron-hole couple and causes the reduction of excited electron-hole recombination [89,90].
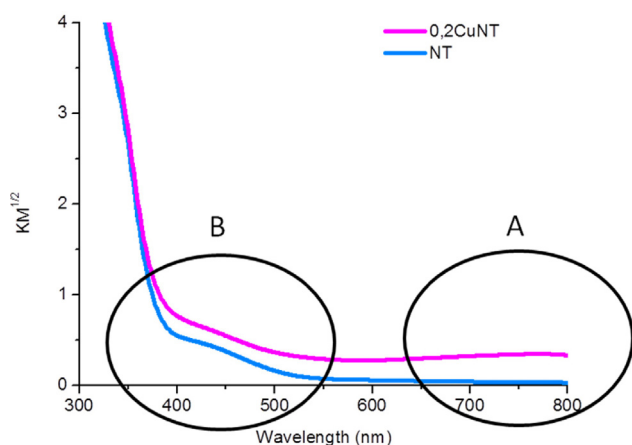
Focusing on the border region between UV and VIS between 350 and 500 nm (section B), the nitrogen band edge persists also in the CuO–TiO_2 sample it is even more intense. In particular 0.2CuNT has shown a higher absorption in this region than NT sample. Moreover, the apparent band gap energies have been calculated and for 0.2CuNT sample this value corresponds to 3.06 eV, which is smaller than the value of pure anatase titania (3.25 eV) and NT (3.16 eV) [91].

Copper does not change the textural features of N promoted TiO_2 photocatalysts: surface area, porous structure and crystalline phase are maintained after CuO addition. The co-catalyst introduction not only preserves N doping effect but, at the same time, significantly improves the catalytic activity reducing electron-hole recombination.

3.3. Effect of copper loading

Afterwards, it has been investigated the effect of copper amount: this can cause variations in the interactions between dopants, co-catalysts and titania, triggering different photoactivity [92].

The copper loading amount (0–0.6 wt.%) has been chosen in accordance with Liu et al. [77] and the real Cu content has been determined by means of FAAS analysis. Catalytic results are shown in Figs. 8 and 9.

The copper amount does not have any effect on catalysts selectivity and, for all samples, methane has been the only product observed.

Comparing reactivity results, it is possible to state that copper effect is not pronounced in 0.1CuNT, while the best catalytic results have been achieved with 0.2CuNT. Then this effect decreases with 0.4CuNT until copper becomes detrimental to photoactivity, like the case of 0.6CuNT. This trend in catalytic behaviour has been observed at any of the investigated reaction times, but it is more evident after six hours reactions.

In order to explain the catalytic performances of the samples, some characterizations have been performed. Titania structural properties are similar in all these samples, as reported in Table 3: surface area values, from N_2 physisorption, range from 93 to 110 m^2/g and XRD patterns show that, anatase is the only observed crystal phase with an average crystalline size of 10 nm. These last data are also confirmed by HRTEM analyses: the average particles size has been determined in the range from 12 to 14 nm for all samples. No copper metal nanoparticles have been detected, even in the sample with the highest amount of this metal.
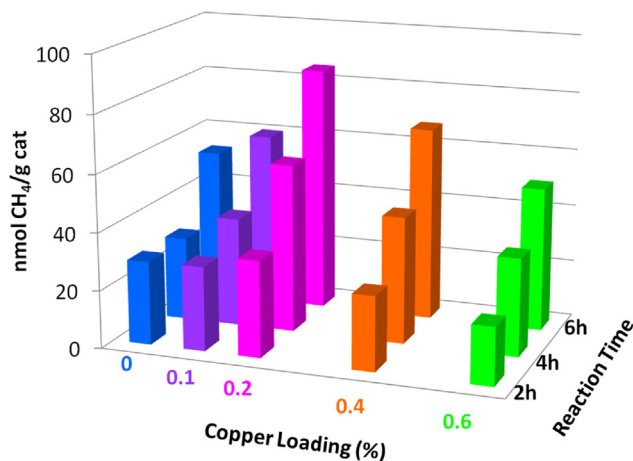

Fig. 7. NT and 0.2CuNT DRS spectra.

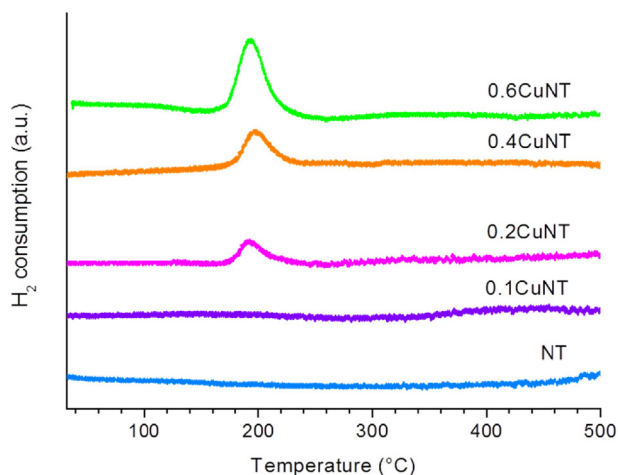**Fig. 8.** Methane production in NT and xCuNT samples containing different amount of copper.

Fig. 9. TPR profiles for NT and xCuNT samples containing different amount of metal.

Table 3
BET surface areas and average pore diameter for NT and CuNT promoted samples.

Sample	Surface area m²/g	Average pore diameter nm
NT	110	17
0.1CuNT	93	20
0.2CuNT	101	14
0.4CuNT	107	24
0.6CuNT	96	15

Table 3 BET surface areas and average pore diameter for NT and CuNT promoted samples. Therefore attention has been put on the nature of the copper using TPR analysis.

Any hydrogen consumption ascribable to reduction species in the NT and 0.1CuNT samples has been observed: both in the NT sample, where there is not copper, and in the 0.1CuNT sample, where copper content is too low to be detected, any reduction has occurred.

In the TPR profiles of the other samples it is possible to observe a band (hydrogen consumption) located at $200 °C$ approximately, that is ascribable to the reduction of Cu^{2+} species to Cu^0. This means that, in all the samples, oxidation state and interaction with titania surface are similar.

In order to understand more deeply the catalytic behaviour, DRS analyses have been performed. In Fig. 10 spectra from NT (the sample doped only with nitrogen), 0.6CuNT (that has the highest amount of copper, 0.6 wt.%) and 0.2CuNT (that has given the best catalytic performances) have been reported.
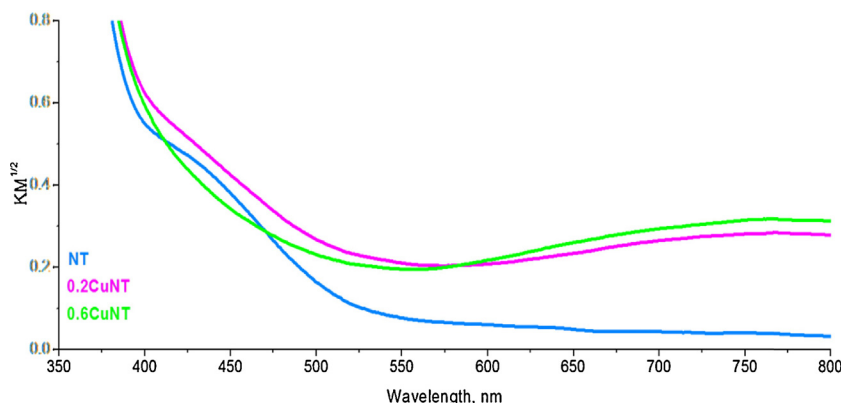
Table 4
Methane and hydrogen production in TONs and selectivity to methane

CO₂/H₂O	CH₄ production TON (nmol$_{CH4}$/g$_{cat}$)	H₂ production TON (nmol$_{H2}$/g$_{cat}$)	Selectivity to CH₄ (%)
13.3	85.3	0	100
10	118.8	6.3	95
5	134.6	7.1	95
2.5	136.9	7.4	94.9
2	139.9	8	94.6
1	92.2	8.8	91.3

By the inspection of the curves, it is possible to single out the following features:

i) in the visible region the broad absorption between 600 and 800 nm for both 0.2CuNT and 0.6CuNT samples is ascribable to the presence of copper oxide species: in particular 0.6CuNT absorption is more intense than that of 0.2CuNT: this difference is due to a greater amount of metal [93].

ii) in the UV–vis border region, between 390 and 480 nm, all the samples present an intense absorption due to nitrogen doping. As already said, copper introduction does not hinder nitrogen effect on titania's light absorption. Among them, in 0.2CuNT band-edge is the most pronounced.

iii) the 0.6CuNT sample presents the worst absorption, indicating a less efficient nitrogen doping effect. This is mainly due to the presence of a great amount of copper which partially covers the titania's surface.

These spectral features are in agreement with the band gap results: as a matter of fact, 0.2CuNT provided the lowest band gap (3.06 eV).

Moreover, it is known that, when copper is present in great amount, Cu species act like recombination centres for photoinduced electron and hole [94,95].

For both these reason there is an optimal balance in copper loading to enhance photoactivity in N doped CuO-TiO₂ photocatalysts [96]. For carbon dioxide photoreduction to methane, the best results have been obtained with a sample containing 0.2 wt.% of copper.

3.4. CO₂/H₂O effect on the products distribution

The last part of the work was addressed to the investigation of the relationship between product distribution and CO_2/H_2O ratios in the feed stream. In fact, CO_2 and H_2O molecules might be competitively activated by the charge transfer of titania excited

Fig. 10. NT, 0.2CuNT and 0.6CuNT DRS spectra.
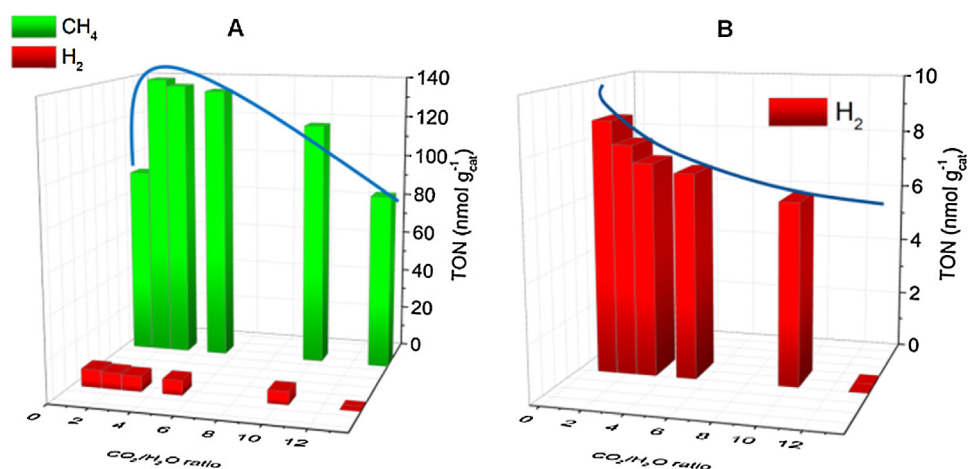
Fig. 11. Trends in methane and hydrogen TON with CO_2/H_2O ratio (A) and hydrogen production in detail (B).

states and the value of CO_2/H_2O ratios could influenced the selectivity for the formation of the products [78,97].

The results of catalytic tests have been reported in Table 4 and in Fig. 11.

The first and most evident consideration is that, decreasing CO_2/H_2O ratio, methane has not been the only detected product, but hydrogen has been formed as well. However, methane has been the predominant product: actually, selectivity to CH_4 stretches between 91.3% and 100%.

Considering methane production only, CO_2/H_2O ratio has had an impact definitely. In particular, decreasing CO_2/H_2O from 13.3 to 2.0 a continuous improvement has been reached with a peak value of 139.9 $nmol_{CH4}/g_{cat}$ at CO_2/H_2O ratio equal to 2.0. Afterwards, when CO_2/H_2O ratio has been further decreased to 1.0, TON has collapsed to 92.2 $nmol_{CH4}/g_{cat}$.

The bell-shaped trend in methane production might be interpreted remembering the presence of two competitive processes. The first one is the necessity of a mutual interaction between the two reactants on the catalyst's surface in order to reduce CO_2. When the amount of CO_2 is low, the interactions between the two reactants is more efficient and we obtain the better catalytic performances.

On the other hand when the CO_2/H_2O ratio is 1.0 or much lower, the main phenomenon is water splitting. In this case water is adsorbed on the photocatalyst more efficiently than CO_2, causing H_2 production and the CH_4 selectivity decrease. The lower CO_2 amount is, the more efficiently CO_2 and H_2O interact one with another, leading to better catalytic performances. Therefore, an optimum H_2O/CO_2 feed ratio could enhance the CO_2 conversion efficiency.

4. Conclusions

Motivated by the two most challenging issues of our society, namely CO_2 pollution and fossil fuels depletion, this work has investigated the N doped Cu-photocatalysts suitable for carbon dioxide photoreduction with water in gas phase in very mild reaction condition. This technology is potentially a winning solution from both the environmental and the energy-efficiency viewpoints.

Through a simple and inexpensive synthetic strategy, the catalytic activity of titania has been improved adding a dopant (N) and a co-catalyst (CuO). In two different ways, both these modifications proved to be effective in upgrading titania catalytic performances. The catalysts selectivity (CH_4, H_2) and productivity

can be controlled by tuning conveniently the reactions conditions. In particular, the CO_2/H_2O ratio is a crucial parameter.

Therefore this work opens the doors to further studies in order to exploit the enormous potentialities of CO_2 photoreduction with water.

References

[1] R.B. Alley, J. Marotzke, W.D. Nordhaus, J.T. Overpeck, D.M. Peteet, R.A. Rielke, R. T. Pierrehumbert, P.B. Rhines, T.F. Stocker, L.D. Talley, J.M. Wallace, Nature 299 (2003) (2005) .
[2] K. Brysse, N. Oreskes, J. O'Reilly, M. Oppenheimer, Global Environ. Change 23 (2013) 327.
[3] K. Stanislawka, K. Krawiec, Z.W. Kundzewicz, Comput. Math. Appl. 64 (2012) 3717.
[4] G.A. Folberth, S.T. Rumbold, W.J. Collins, T.M. Butler, Urban Climate 1 (2012) 4.
[5] E. Benhal, G. Zahedi, E. Shamsaei, A. Bahadori, J. Cleaner Prod 51 (2013) 142.
[6] IEA, Redrawing the energy-climate map: World Energy Outlook Special Report, available on http://www.iea.org
[7] J.G.J. Olivier, G. Janssens-Maenhout, M. Muntean, J.A.H.W. Peters, 2013. Trends in Global CO2 emissions: 2013 Report, 1st ed. PBL 2013 The Hague The Netherland.
[8] H. Arawaka, M. Aresta, J.N. Armor, M.A. Barteau, E.J. Beckman, A.T. Bell, J.E. Bercaw, C. Creutz, E. Dinjus, D.A. Dixon, K. Domen, D.L. Dubois, J. Eckert, E. Fujita, D.H. Gibson, W.A. Goddard, D.W. Goodman, J. Keller, G.J. Kubas, H.H. Kung, J.E. Lyons, L.E. Manzer, T.J. Marks, K. Morukuma, K.M. Nicholas, R. Periana, L. Que, J. Rostrup-Nielsen, W.M.H. Sachter, L.D. Schmidt, A. Sen, G.A. Somorjai, P.C. Star, B.R. Stults, W. Tumas, Chem. Rev. 101 (2001) 953.
[9] G. Centi, S. Perathoner, Catal. Today 148 (2009) 191.
[10] K. Kalyanasundaram, M. Graetzel, Curr. Opin. Biotechnol. 21 (2010) 298.
[11] C. Graves, S.D. Ebbesen, M. Morgensen, K.S. Lackner, Renew. Sust. Energ. Rev. 15 (2011) 1.
[12] R. De Richter, S. Caillol, J. Photochem. Photobiol. C 12 (2011) 1.
[13] G. Centi, S. Perathoner, Chemsuschem 3 (2010) 195.
[14] S. Abanades, H.I. Villafan-Vidales, Chem. Eng. J. 175 (2011) 368.
[15] V.P. Indrakanti, J.D. Kubicki, H.H. Schobert, Energy Environ. Sci. 2 (2009) 745.
[16] J. Hong, W. Zhang, J. Ren, R. Xu, Anal. Methods 5 (2013) 1086.
[17] S.N. Habisreutinger, L. Schmidt-Mende, J.K. Stolarczyk, Angew. Chem. Int. Ed. 52 (2013) 7372.
[18] A. Corma, H. Garcia, J. Catal. 308 (2013) 168.
[19] A. Dhakshinamoorthy, S. Navalon, A. Corma, H. Garcia, Energy Environ. Sci. 5 (2012) 9217.
[20] Y. Izumi, Coord. Chem. Rev. 257 (2013) 171.
[21] K. Mori, H. Yamashita, M. Anpo, RSC Adv. 2 (2012) 3165.
[22] T. Ohno, K. Sarukawa, K. Tokieda, M. Matsumura, J. Catal. 203 (2001) 82.
[23] R. Zhang, Y. Bai, B. Zhang, L. Chen, B. Yan, J. Hazard. Mater. 211–212 (2012) 404.
[24] S. Hackenberg, G. Friehs, K. Froelich, C. Ginzkey, C. Koehler, A. Scherzed, M. Urghartz, R. Hagen, N. Kleinsasser, Toxicol. Lett. 195 (2010) 9.
[25] X. Chen, S.S. Mao, Chem. Rev. 107 (2007) 2891.

[26] M.R. Hoffmann, S.T. Martin, W. Choi, D.W. Bahneman, Chem. Rev. 95 (1995) 69.
[27] A.L. Linsebigler, G. Lu, J.T. Yates, Chem. Rev. 95 (1995) 735.
[28] M. Li, M.K.H. Leung, D.Y.C. Leung, K. Sumathy, Renew. Sust. Energ. Rev. 11 (2007) 401.
[29] W.K. Jo, J.H. Park, H.D. Chun, J. Photochem. Photobiol. A 148 (2002) 109.
[30] S. Wang, H.M. Ang, M.O. Tade, Environ. Int. 33 (2007) 694.
[31] M. Signoretto, E. Ghedini, V. Trevisan, C.L. Bianchi, M. Ongaro, G. Cruciani, Appl. Catal. B 95 (2010) 130–136.
[32] V. Trevisan, M. Signoretto, F. Pinna, G. Cruciani, G. Cerrato, Chem. Today 30 (2012) 25.
[33] V. Trevisan, A. Olivo, F. Pinna, M. Signoretto, F. Vindigni, G. Cerrato, C.L. Bianchi, Appl. Catal. B 160 (2014) 152.
[34] T. Inoue, A. Fujishima, S. Konishi, K. Honda, Nature 277 (1979) 637.
[35] A. Fujishima, K. Honda, Nature 238 (1972) 37.
[36] H.Y. He, P. Zapol, L.A. Curtiss, J. Phys. Chem. 114 (2010) 21474.
[37] H.Y. He, P. Zapol, L.A. Curtiss, Energy Environ. Sci. 5 (2012) 6196.
[38] S.S. Tan, L. Zou, E. Hu, Catal. Today 11 (2006) 269.
[39] G. Liu, N. Hoivik, K. Wang, H. Jakobsen, Sol. Energ. Mater. Sol C 105 (2012) 53.
[40] L. Schmidt-Mende, J.K. Stolarczyk, S.N. Habisreutinger, Agew. Chem. Int. Ed. 52 (2013) 7372.
[41] A.J. Cowan, J. Tang, W. Leng, J.R. Durrant, D.R. Klug, J. Phys. Chem. C 114 (2010) 4208.
[42] L. Artiglia, D. Lazzari, S. Agnoli, G.A. Rizzi, G. Granozzi, J. Phys. Chem. C 117 (2013) 13163.
[43] V. Trevisan, E. Ghedini, M. Signoretto, F. Pinna, C.L. Bianchi, Microchem. J. 112 (2014) 186.
[44] Y. Yin, W. Zhang, S. Chen, S. Yu, Mater. Chem. Phys. 113 (2009) 982–985.
[45] M.V. Dozzi, B. D'Andrea, G. Valentini, E. Selli, J. Phys. Chem. C 117 (2013) 25586.
[46] L. Verèb, A. Oszkò, A. Sienkiewicz, K. l. Forrò. Mogyoròsi, A. Dombi, K. Hernàdi, Appl. Catal. B 129 (2013) 194.
[47] M.V. Dozzi, E. Selli, J. Photochem. Photobiol. 14 (2013) 13 C.
[48] L. Gomathi Devi, R. Kavitha, Appl. Catal. B 140–141 (2013) 559.
[49] R. Asahi, T. Moriwaka, T. Ohwaki, K. Aoki, Y. Taga, Science 293 (2001) 269.
[50] J.J. Murcia, J.A. Naviò, M.C. Hidalgo, Appl. Catal. B 126 (2012) 76.
[51] Q. Lu, Z. Lu, Y. Lu, L. Lu, Y. Ning, H. Yu, Y. Hou, Y. Yin, Nano Lett. 13 (2013) 5698.
[52] J.A. Anderson, Catal. Today 181 (2012) 171.
[53] A. Primo, A. Corma, H. García, Phys. Chem. Chem. Phys. 13 (2011) 886.
[54] J. Choi, H. Park, M.R. Hoffmann, J. Phys. Chem. C 114 (2010) 783–792.
[55] A. Fuerte, M.D. Hernandez-Alonso, A.J. Maira, A. Martinez-Arias, M. Fernandez-Garcia, J.C. Conesa, J. Soria, Chem. Commun 24 (2001) 2718.
[56] W.N. Wang, J. Soulis, Y.J. Yang, P. Biswas, Aerosol Air Qual. Res. 14 (2014) 533.
[57] Y. Li, W.N. Wang, Z.L. Zhan, M.H. Woo, C.Y. Wu, P. Biswas, Appl. Catal. B 100 (2010) 386.
[58] K. Lalitha, G. Sadanandam, V.D. Kumari, M. Subrahmanyam, B. Sreedhar, N.Y. Hebalkar, J. Phys. Chem. C 114 (2010) 22181.
[59] S. Chu, X.M. Zheng, F. Kong, G.H. Wu, L.L. Luo, Y. Guo, H.L. Liu, Y. Wang, H.X. Yu, Z.G. Zou, Mater. Chem. Phys. 129 (2011) 1184.
[60] Y.H. Xu, D.H. Liang, M.L. Liu, D.Z. Liu, Mater. Res. Bull. 43 (2008) 3474.
[61] H.X. Li, Z.F. Bian, J. Zhu, Y.N. Huo, H. Li, Y.F. Lu, J. Am. Chem. Soc. 129 (2007) 4538.

[62] S. Krejcikova, L. Matejova, K. Koci, L. Obalova, Z. Matej, L. Capek, O. Solcova, Appl. Catal. B 111–112 (2012) 119–125.
[63] T. Nguyen, J.C.S. Wu, Appl. Catal. A 335 (2008) 112.
[64] H. Sun, G. Zhou, S. Liu, H.M. Ang, M.O. Tadé, S. Wang, Chem. Eng. J. 231 (2013) 18.
[65] X.K. Li, Z.J. Zhuang, W. Li, H.Q. Pan, Appl. Catal. A 429 (2012) 31.
[66] W. Kim, T. Tachikawa, H. Kim, N. Lakshminarasimhan, P. Murugan, H. Park, T. Majima, W. Choi, Appl. Catal. B 147 (2014) 642.
[67] X.A. Li, M. Khraisheh, J. Tang, Catal. Today 224 (2014) 3.
[68] P. Usubharatana, D. McMartin, A. Veawab, P. Tontiwachwuthikul, Ind. Eng. Chem. Res. 45 (2006) 2558.
[69] M. Anpo, H. Yamashita, Y. Ichihashi, S. Ehara, J. Electroanal. Chem. 336 (1995) 21.
[70] A. Dhakshinamoorthy, S. Navalon, A. Corma, H. Garcia, Energy Environ. Sci. 5 (2012) 9217.
[71] M. Tahir, N.S. Amin, Chem. Eng. J. 230 (2013) 314.
[72] M. Tahir, N.S. Amin, Appl. Catal. B 162 (2015) 98.
[73] M.A. Tabatabai, Environ. Lett. 7 (1974) 237.
[74] S. Brunauer, P.H. Emmett, E. Teller, J. Am. Chem. Soc. 60 (1938) 309.
[75] E.P. Barrett, l.G. Joyner, P.P. Halenda, J. Am. Chem. Soc. 73 (1951) 373.
[76] P. Kubelka, F. Munk, Z. Tech. Phys. 12 (1931) 593–601.
[77] D. Liu, Y. Fernández, O. Ola, S. Mackintosh, M. Varoto-Valer, C.M.A. Parlett, A.F. Lee, J.C.S. Wu, Catal. Commun. 25 (2012) 78.
[78] M. Tahir, N.S. Amin, Appl. Catal. B 142–143 (2013) 512.
[79] U. Diebold, Surf. Sci. Rep. 48 (2003) 53.
[80] A. Kubacka, M. Fernández-García, G. Colón, Chem. Rev. 112 (2012) 1555.
[81] www.eurosupport.nl.
[82] R. Asahi, T. Moriwaka, T. Ohwaki, K. Aoki, Y. Taga, Science 293 (2001) 269.
[83] Y. Yin, W. Zhang, S. Chen, S. Yu, Mater. Chem. Phys. 113 (2009) 982.
[84] T. Shibata, H. Irie, M. Ohmori, A. Nakajima, T. Watanabe, K. Hashimoto, Phys. Chem. Chem. Phys. 6 (2004) 1359.
[85] M. Ni, M.K.H. Leung, D.Y.C. Leung, K. Sumathy, Renew. Sust. Energ. Rev. 11 (2007) 401.
[86] E.E. Benson, C.P. Kubiak, A.J. Sathrum, J.M. Smieja, Chem. Soc. Rev. 38 (2009) 89.
[87] J.C.S. Wu, H.M. Linì, C.L. Lai, Appl. Catal. A 296 (2005) 194.
[88] S. Ghasemi, A. Esfandiar, S. Rahman Setayesh, A. Habibi-Yangjeh, A. Irajizad, Appl. Catal. A 462 (2013) 82.
[89] A. Zaleska, A. Nischk, A. Cybula, New and Future Developments in Catalysis—Solar Photocatalysis, in: S.L. Suib (Ed.), Elsevier, 2013, pp. 63–102.
[90] L.S. Yoong, F.K. Chong, B.K. Dutta, Energy 34 (2009) 1652.
[91] J. Zhang, Y. Wu, M. Xing, S.H.K. Leghari, S. Saijad, Energy Environ. Sci 3 (2010) 715.
[92] L. Liu, F. Gao, H. Zhao, Y. Li, Appl. Catal. B 134 (2013) 349.
[93] J. Yu, Y. Hai, M. Jaroniec, J. Colloid Interface Sci. 357 (2011) 223.
[94] B. Xin, P. Wang, D. Ding, J. Liu, Z. Ren, H. Fu, Appl. Surf. Sci. 254 (2008) 2569.
[95] K. Song, J. Zhou, J. Bao, Y. Feng, J. Am. Ceram. Soc. 91 (2008) 1369.
[96] S. Qin, F. Xin, Y. Liu, X. Yin, W. Ma, J. Colloid Interface Sci. 365 (2011) 257.
[97] K. Ikeue, S. Nozaki, M. Ogawa, M. Anpo, Catal. Today 74 (2002) 241.